

NUMERICAL SOLUTIONS TO POISSON'S EQUATION  
OVER NON-UNIFORM DISCRETIZATIONS WITH  
ASSOCIATED FAST SOLVERS

by

Richard J. Clancy

A thesis submitted to the Graduate College of  
Texas State University in partial fulfillment  
of the requirements for the degree of  
Master of Science  
with a Major in Applied Mathematics  
May 2017

Committee Members:

Young Ju Lee, Chair

Gregory Passty

Ray Treinen

**COPYRIGHT**

by

Richard J. Clancy

2017

## **FAIR USE AND AUTHOR'S PERMISSION STATEMENT**

### **Fair Use**

This work is protected by the Copyright Laws of the United States (Public Law 94-553, section 107). Consistent with fair use as defined in the Copyright Laws, brief quotations from this material are allowed with proper acknowledgement. Use of this material for financial gain without the author's express written permission is not allowed.

### **Duplication Permission**

As the copyright holder of this work I, Richard J. Clancy, authorize duplication of this work, in whole or in part, for educational or scholarly purposes only.

## ACKNOWLEDGEMENTS

There are many people to thank for making my time at Texas State University a productive, enjoyable experience. I would like to thank Dr. Young Ju Lee for the countless hours spent discussing our research. These conversations were often fruitful and always entertaining. Dr. Lee encouraged me when I was down and freely shared his insight when difficulties arose. I would also like to thank my committee, Dr. Gregory Passty and Dr. Ray Treinen, who were gracious enough to read through my thesis in its rough form; an arduous task. I would also like to thank my many office-mates, Esther Conrad, Erika Gallo, Terra Hyde, Nathan "Steve" Jones, Josh Rice, Ellen Robinson, Robert Salit, and Martin Schmidt for making the hours spent between classes a highlight of my time at Texas State. I am deeply grateful to my family for their love and support throughout my life; I cannot imagine where I would be without them. Last but certainly not least, I want to thank my exceptional wife, Mina, who encouraged me to pursue my passion and shouldered many of the responsibilities I neglected as a graduate student. This thesis would not be possible without her.

## TABLE OF CONTENTS

	Page
ACKNOWLEDGEMENTS . . . . .	iv
LIST OF TABLES . . . . .	vi
LIST OF FIGURES . . . . .	vii
ABSTRACT . . . . .	viii
CHAPTER	
I. INTRODUCTION . . . . .	1
II. THEORY . . . . .	4
II.1 Extension to Interior Non-Uniformities . . . . .	6
II.2 Prior Results . . . . .	7
II.3 New Mesh Function and Inequality for $R_h^*$ . . . . .	15
II.4 Error over General Domain with Non-Uniform Interior Mesh . . . . .	21
II.5 Remarks Considering Growth of $O_X$ and $O_Y$ . . . . .	23
III. NUMERICAL SOLUTIONS AND FAST SOLVERS . . . . .	26
III.1 Basic Solvers . . . . .	27
III.2 The Multigrid Method . . . . .	28
III.3 Limitations of the Multigrid Method for Graded Meshes . . . . .	31
IV. FUTURE WORK . . . . .	34
REFERENCES . . . . .	35

## LIST OF TABLES

Table		Page
II.1	Growth of $O_X$ and $O_Y$ . . . . .	24
III.1	Solution time in seconds for different methods . . . . .	31
III.2	Node placement for different $\kappa$ values . . . . .	31
III.3	Asymptotic convergence rates and number of iterations for various $\kappa$ . . . . .	32
III.4	Aspect Ratio and min/max step-size after 10 refinements . . . . .	33

## LIST OF FIGURES

Figure		Page
I.1	Usual discretization and a refinement . . . . .	2
I.2	Approximate solution to system (left), error profile (right) . . . . .	2
I.3	A graded adaptive mesh through several refinements . . . . .	3
II.1	Circular domain with non-uniformities at boundary adjacent nodes . . . . .	6
II.2	Example of the mesh function $Z(x, y)$ . . . . .	17
II.3	Plot of $x$ vs. $Z(x, 0)$ . . . . .	18
III.1	Evolution of Gauss-Seidel smoothing: every 25 <sup>th</sup> iterate plotted . . . . .	28
III.2	Evolution of multigrid solver: every iterate plotted . . . . .	30
III.3	Oscillations arising from highly irregular discretizations . . . . .	33

## ABSTRACT

Partial differential equations (PDE's) lay the foundation for the physical sciences and many engineering disciplines. Unfortunately, most PDE's can't be solved analytically. This limitation necessitates approximate solutions to these systems. This thesis focuses on a particular formulation for solving differential equations numerically known as the finite difference method (FDM). Traditional FDM calls for a uniform discretization of the domain over which the PDE is defined. In certain cases, the behavior of a PDE's solution is interesting in a particular region that we would like to better understand. Uniform discretization fails to increase resolution where desired. This manuscript investigates the approximation error of non-uniform discretizations and outlines attempts made at developing a fast-solver for efficiently handling the resultant non-symmetric system of linear equations.

## I. INTRODUCTION

Physicists, chemists, and engineers have long used differential equations (DE's) to understand the world and advance technology. In recent years, a growing number of fields including biology and the social sciences have begun developing their own DE's to analyze populations and make predictions. This interest has opened a variety of new and exciting problems to mathematicians.

Along with the desire to bring mathematical rigor to other disciplines comes strong demand for techniques that solve the associated equations. Unfortunately, most DE's are extremely difficult if not impossible to solve. As a result, there is a growing need for computational methods to deal with these troublesome equations. One such scheme is the finite difference method (FDM) which solves DE's numerically. The method involves reducing a continuum to a finite number of points, or unknowns, and devising a difference equation that approximates the original differential form. The FDM gives rise to a system of linear equations that are then solved for each unknown. Intermediate values are interpolated allowing for an approximate solution over the domain. A standard uniform discretization guarantees an  $O(h^2)$  approximation where  $h$  is the step-size or distance between any node and its neighbors. If  $u$  is the exact solution and  $U$  is approximate, then  $U = u + O(h^2)$ . In other words, when the step-size is halved, the error of the approximation drops by a factor of four.

In order for numerical approximations to be useful, their error must be below a given tolerance. Suitable levels of precision are normally ensured by increasing resolution, i.e. solving the system at more points. For many applications, engineers and scientists require a level of accuracy corresponding to one million unknowns. Increased accuracy comes with a heavy computational cost; an entry level laptop running a basic algorithm can take days to solve a system of this size.

Traditionally, a domain is discretized by overlaying it with a uniform grid. The intersection of grid-lines, called nodes, represent locations at which the equation will be solved. When increased accuracy is desired, new grid-lines are placed at the midpoints of existing

nodes, a process known as mesh refinement. A uniform mesh and its refinement is shown in Figure I.1. Uniform meshes are popular since they are easy to implement and give rise to symmetric systems of equations which are well understood mathematically. For smooth, well-behaved functions, this works fine, but not all DE's benefit from this democratic increase of resolution.

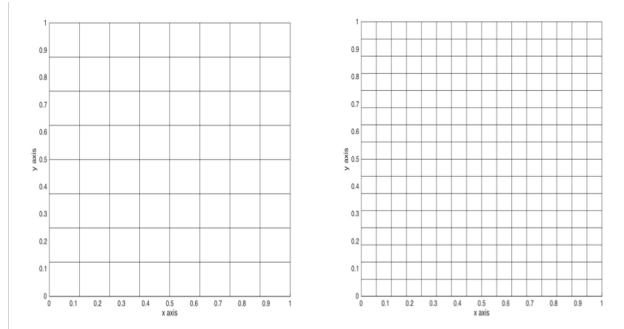


Figure I.1: Usual discretization and a refinement

Take for instance the differential equation given by

$$\begin{cases} \Delta u(x, y) = -1 & \text{in } \Omega \\ u(x, y) = 0 & \text{on } \partial\Omega, \end{cases} \quad (\text{I.1})$$

where

$$\bar{\Omega} = \Omega \cup \partial\Omega = \{[0, 1] \times [0, 1]\} \setminus \{[0, 1/2) \times (1/2, 1]\}. \quad (\text{I.2})$$

Simply stated,  $\Omega$  is the interior of a flag shaped domain with a reentrant corner at  $(1/2, 1/2)$  and  $\partial\Omega$  is the domain's boundary. The numerical solution to the above system can be seen in Figure I.2 along with the error profile of the approximate solution over the domain.

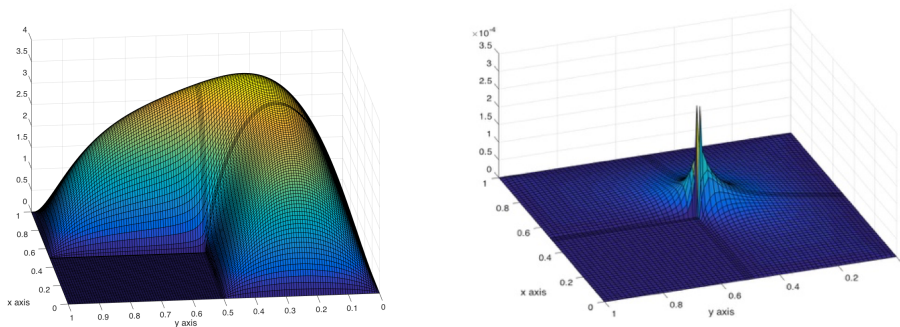


Figure I.2: Approximate solution to system (left), error profile (right)

The solution's derivative around the reentrant corner at  $(1/2, 1/2)$  changes rapidly and is responsible for the largest error of the system. This can be seen graphically by the right surface of Figure I.2. Values throughout the rest of the domain quickly converge to the true solution, but error at the reentrant corner remains stubbornly high. It would be advantageous to "zoom-in" on the interior corner and investigate local behavior more closely. One method is the employment of an adaptive mesh refinement scheme. Octotree and graded meshes are among the most popular. In this paper, we limit our discussion to graded adaptive meshes. An example of a graded mesh and several refinements is shown in Figure I.3.

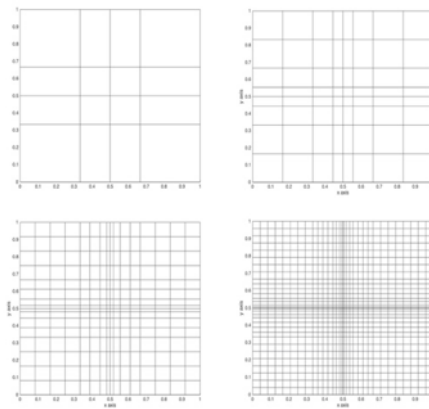


Figure I.3: A graded adaptive mesh through several refinements

Unfortunately a five-point stencil on a non-uniform grid no longer guarantees an  $O(h^2)$  approximation; it only guarantees an  $O(h)$  approximation. This theoretical reduction of accuracy is a cause for concern and has driven many away from FDM to more cumbersome numerical schemes such as the finite element method.

Despite this loss in theoretical accuracy, numerical experiment shows that non-uniform discretizations still result in  $O(h^2)$  approximations. A proof for this fact is provided in Chapter II which is the primary theoretical contribution of this paper. In addition, a description of the multigrid (MG) method is provided in Chapter III followed by our attempts at generalizing MG to solve the resultant system of linear equations for non-uniform discretizations.

## II. THEORY

Throughout this thesis, we use  $P \in \mathbb{R}^2$  rather than  $(x, y) \in \mathbb{R}^2$  when convenient. We begin by considering Poisson's equation with Dirichlet boundary conditions

$$\begin{cases} \Delta u(P) = F(P), & P \in \Omega \\ u(P) = f(P), & P \in \partial\Omega, \end{cases} \quad (\text{II.1})$$

where  $\Omega$  is the interior of a domain,  $\partial\Omega$  is its boundary, and  $\bar{\Omega} = \Omega \cup \partial\Omega$ . The function  $F(P)$  and  $f(P)$  are given and  $u(P)$  is the solution we seek.

In many applications, it is sufficient to solve the above equation approximately by discretizing the domain in question. This is accomplished by applying a grid over the domain and solving the system at the intersection of grid-lines called nodes. The uniform discretization of a square domain and one refinement is shown in Figure I.1. By devising a finite difference analogue through the use of Taylor Series expansions, the solution can be approximated over all nodes with the discrete operator  $\Delta_h$ . Our goal is then to solve

$$\begin{cases} \Delta_h U(P) = F(P), & P \in \Omega_h \\ U(P) = f(P), & P \in \partial\Omega_h, \end{cases} \quad (\text{II.2})$$

where  $\Omega_h$  is the set of all interior nodes and  $\partial\Omega_h$  is the set of all boundary nodes. Note that  $\Omega_h \subset \Omega$  and  $\partial\Omega_h \subset \partial\Omega$ . Here,  $U(P)$  is the approximate solution to the original problem. The discrete operator,  $\Delta_h$ , can be represented as a square matrix. It has been established in [2] that this system matrix has a non-zero determinant. By the Invertible Matrix Theorem, the matrix has an inverse and therefore a unique solution.

In the case of a uniform mesh on a rectangular domain, the discrete operator is given by

$$\begin{aligned} \Delta_h U(x, y) = & \frac{1}{h^2} \{U(x+h, y) + U(x-h, y) \\ & + U(x, y+h) + U(x, y-h) - 4U(x, y)\}, \end{aligned} \quad (\text{II.3})$$

where  $h$  is the mesh spacing and  $(x, y) \in \bar{\Omega}_h = \Omega_h \cup \partial\Omega_h$ . It is well known that the above difference equation for uniform meshes provides an optimal  $O(h^2)$  approximation and satisfies the following inequality

$$|\Delta u(P) - \Delta_h u(P)| \leq \frac{h^2}{6} M_4, \quad (\text{II.4})$$

with  $M_i = \sup_{P \in \Omega} \{ |\frac{\partial^i u(P)}{\partial^j x \partial y^{i-j}}| \mid j = 0, 1, \dots, i \}$ .

When discussing non-uniform meshes, the discrete operator must be revised to achieve the desired cancellations of leading terms in the Taylor series expansion. The revised discrete operator originally proposed in [4] is known as the Shortley-Weller Equation (SWE) and given by

$$\begin{aligned} \Delta_h U(x, y) = & \frac{2}{h^2} \left\{ \frac{U(x + eh, y)}{e(e + w)} + \frac{U(x - wh, y)}{w(e + w)} \right. \\ & \left. + \frac{U(x, y + nh)}{n(n + s)} + \frac{U(x, y - sh)}{s(n + s)} - U(x, y) \left( \frac{1}{ew} + \frac{1}{ns} \right) \right\}, \end{aligned} \quad (\text{II.5})$$

where  $0 < n, s, e, w \leq 1$  are proportions of the largest mesh size  $h$  to the next node in their corresponding cardinal direction (e.g.  $n$  corresponds with north towards the top of page). It is easy to see that when  $n = s = e = w = 1$ , the discrete operator reduces to (II.3). The above discretization of  $\Delta$  satisfies the following inequality

$$|\Delta u(P) - \Delta_h u(P)| \leq \frac{2M_3}{3} h, \quad (\text{II.6})$$

which indicates that the SWE only guarantees an  $O(h)$  approximation. In other words, it is no longer an optimal approximation for a 5-point stencil.

This theoretically suboptimal convergence was a cause for concern. If there existed a single non-uniformity in the mesh,  $2^{\text{nd}}$  order convergence could be lost. PDE's defined over irregular domains suffered. It seemed that domains as simple as the circular one shown in Figure II.1 were doomed to suboptimal convergence.

Despite this seeming  $O(h)$  approximation, numerical experiments painted another picture. Regardless of boundary geometry, domains with non-uniformities restricted to boundary adjacent nodes continued to exhibit  $2^{\text{nd}}$  order convergence. In [1], Bramble and Hubbard investigated the error of the SWE over a mesh with non-uniformities along the bound-

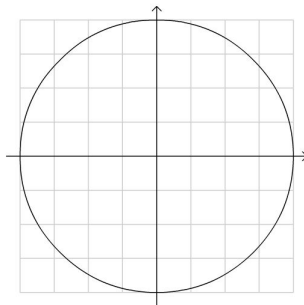


Figure II.1: Circular domain with non-uniformities at boundary adjacent nodes

ary interface (points where at least one neighbor belongs to  $\partial\Omega_h$ ). They went on to show that the error,  $\varepsilon$ , between the exact and approximate solution is bounded by

$$|\varepsilon(P)| \leq \frac{M_4 d^2}{96} h^2 + \frac{2M_3}{3} h^3, \quad P \in \Omega, \quad (\text{II.7})$$

where  $d$  is the diameter of the smallest circumscribed circle containing  $\Omega$ . Their result established that uniform meshes can be applied to irregular domains without a loss in the order of convergence despite employment of the SWE at boundary adjacent nodes where non-uniformities are present. Their result neatly cleared up the issues for domains with complex geometries including simple cases like the circular domain of Figure II.1.

### II.1 Extension to Interior Non-Uniformities

As motivated in Chapter I, it is desirable to selectively enhance resolution in certain regions such as the neighborhood around the reentrant corner of Figure I.2. Although Bramble and Hubbard's result establishes a global  $O(h^2)$  approximation for the 5-point finite difference scheme over domains with complex geometries, it does not permit non-uniformity to be extended throughout the interior. In this chapter, a proof is given showing that a completely non-uniform discretization can be extended to the interior of any domain without a loss in the rate of convergence. In particular, it will be shown that

$$|\varepsilon(P)| \leq \frac{2h^2}{3} \left\{ \frac{D^2 M_4}{64} + M_3 \left[ h + \frac{d_x + d_y}{(O_X^2 + O_X)^{-1} + (O_Y^2 + O_Y)^{-1}} \right] \right\}, \quad P \in \Omega \quad (\text{II.8})$$

where

$h$	maximum step-size over $\bar{\Omega}_h$ ,
$M_i$	largest value of $i^{th}$ derivative in $\bar{\Omega}$ ,
$D$	diameter of smallest circle circumscribing $\Omega$ ,
$d_x$	$\max\{x \mid (x, y) \in \bar{\Omega}\} - \min\{x \mid (x, y) \in \bar{\Omega}\}$ ,
$d_y$	$\max\{y \mid (x, y) \in \bar{\Omega}\} - \min\{y \mid (x, y) \in \bar{\Omega}\}$ ,
$O_X, O_Y$	number of non-uniformities in the $x$ and $y$ directions respectively.

Instrumental to our proof is the introduction of a finite difference analogue to Green's function,  $G_h(P, Q)$ , defined by

$$\begin{cases} \Delta_{h,P} G_h(P, Q) &= -\frac{\delta(P,Q)}{h^2}, & P \in \Omega_h \\ G_h(P, Q) &= \delta(P, Q), & P \in \partial\Omega_h, \end{cases} \quad (\text{II.9})$$

with  $\delta(P, Q)$  as the Kronecker delta defined in its normal sense as

$$\delta(P, Q) = \begin{cases} 1, & P = Q \\ 0, & P \neq Q. \end{cases} \quad (\text{II.10})$$

In an effort to clarify the motivation for each lemma, it is instructive to provide an outline of the following proof. A maximum principle is established to allow for an alternative representation of any function defined over  $\bar{\Omega}_h$  which will be referred to as a mesh function from this point forward. This representation can be thought of as a discretized version of Green's Third Identity. We recast our error mesh function in this form, then focus on establishing upper and lower bounds on the discrete Green's function. We then use these results to establish an upper bound on the absolute value of the error.

## II.2 Prior Results

This section provides results from [1] used in our proof. Some lemmas require slight modifications due to the use of a non-uniform mesh.

**Lemma 1** (Maximum Principle). *For any mesh function,  $V(P)$ , defined on  $\Omega_h \cup \partial\Omega_h$ , if  $\Delta_h V(P) \geq 0$ ,  $\forall P \in \Omega_h$ , then  $V_{\max}(P) \in \partial\Omega_h$ .*

*Proof.* Assume for the sake of contradiction that  $\Delta_h V(x, y) \geq 0 \forall (x, y) \in \Omega_h$  and that the maximum value of  $V(x, y)$  over  $\bar{\Omega}_h$  occurs on the interior at  $(x_0, y_0) \in \Omega_h$ . Let  $V_e, V_w, V_n$ , and  $V_s$  be function values at neighboring points  $(x_0 + eh, y_0)$ ,  $(x_0 - wh, y_0)$ ,  $(x_0, y_0 + nh)$ , and  $(x_0, y_0 - sh)$  respectively and  $V_0 = V(x_0, y_0)$ .

Applying the discrete operator (II.5) to  $V_0$  and rearranging terms we have

$$0 \leq \frac{wV_e + eV_w - (e + w)V_0}{ew(e + w)} + \frac{sV_n + nV_s - (n + s)V_0}{ns(n + s)}.$$

Letting  $V_B = \max\{V_e, V_w, V_n, V_s\}$  then

$$\begin{aligned} 0 &\leq \frac{wV_e + eV_w - (e + w)V_0}{ew(e + w)} + \frac{sV_n + nV_s - (n + s)V_0}{ns(n + s)} \\ &\leq \frac{(e + w)V_B - (e + w)V_0}{ew(e + w)} + \frac{(n + s)V_B - (n + s)V_0}{ns(n + s)} \\ &= \frac{V_B - V_0}{ew} + \frac{V_B - V_0}{ns}. \end{aligned}$$

Letting  $a = \min\{e, w, n, s\} > 0$ , we know the following inequality holds

$$\begin{aligned} 0 &\leq \frac{2V_B - 2V_0}{a^2} \\ \implies 0 &\leq V_B - V_0. \end{aligned}$$

Since  $V_0$  is the maximum, then  $0 \leq V_B - V_0 \leq 0$ . This implies that  $V(x, y)$  is a constant function thus the maximum occurs at the boundary as well. If  $V(x, y)$  is not constant, then we arrive at a contradiction. Hence, the maximum must occur on the  $\partial\Omega_h$ .  $\square$

Although Bramble and Hubbard offer proofs of Lemmas 2, 4, and 5, we include proofs below for the sake of completeness.

**Lemma 2.** Let  $V(P)$  be any mesh function defined on  $\bar{\Omega}_h$ . Then for  $P \in \bar{\Omega}_h$

$$V(P) = h^2 \sum_{Q \in \Omega_h} G_h(P, Q)[- \Delta_h V(Q)] + \sum_{Q \in \partial \Omega_h} G_h(P, Q)V(Q). \quad (\text{II.11})$$

*Proof.* Let the right hand side of the equation equal  $W(P)$ . When  $P \in \partial \Omega_h$ , the first summation drops since it sums over  $\Omega_h$  such that  $P \neq Q$  for any  $Q$ . Focusing on the second term, summing over the boundary will generate a contribution only when  $P = Q$  with remaining terms equaling zero. Using the definition of the delta function,  $W(P) = V(P)$  when  $P \in \partial \Omega_h$ .

When  $P \in \Omega_h$  the second term drops since it only contributes when  $P \in \partial \Omega$  leaving  $W(P) = h^2 \sum_{Q \in \Omega_h} G_h(P, Q)[- \Delta_h V(Q)]$ . Applying the discrete operator to  $W(P)$  at point  $P$  we have

$$\Delta_h W(P) = \Delta_{h,P} W(P) = h^2 \sum_{Q \in \Omega_h} \Delta_{h,P} G_h(P, Q)[- \Delta_h V(Q)].$$

Since  $G_h(P, Q)$  is the only factor with a dependence on  $P$ , we may operate on it alone such that

$$\begin{aligned} \Delta_{h,P} W(P) &= h^2 \sum_{Q \in \Omega_h} [\Delta_{h,P} G_h(P, Q)][- \Delta_h V(Q)] \\ &= h^2 \sum_{Q \in \Omega_h} \left( \frac{-\delta(P, Q)}{h^2} \right) [- \Delta_h V(Q)] = \Delta_h V(P) \end{aligned}$$

Thus we have

$$\begin{aligned} \Delta_h W(P) &= \Delta_h V(P), & P \in \Omega_h \\ W(P) &= V(P), & P \in \partial \Omega_h. \end{aligned}$$

We know that  $\Delta_h$  can be represented as an invertible matrix and therefore has a unique solution; this implies that  $V(P) = W(P)$ . Hence the right hand side equals the left hand side of (II.11) which concludes the proof.  $\square$

**Lemma 3.** *The error function  $\varepsilon(P) = U(P) - u(P)$ , where  $u(P)$  and  $U(P)$  are solutions to (II.1) and (II.23) respectively, is bounded by*

$$|\varepsilon(P)| \leq h^2 \sum_{Q \in \Omega_h} \left| G_h(P, Q) \right| \left| \Delta_h u(Q) - \Delta u(Q) \right|. \quad (\text{II.12})$$

*Proof.* By Lemma 2,

$$\varepsilon(P) = h^2 \sum_{Q \in \Omega_h} G_h(P, Q) [-\Delta_h \varepsilon(Q)] + \sum_{Q \in \partial \Omega_h} G_h(P, Q) \varepsilon(Q), \quad \forall P \in \Omega_h. \quad (\text{II.13})$$

The solution's boundary values are known, hence  $\varepsilon(P) = 0 \forall P \in \partial \Omega_h$  and the second summation equals zero. Since  $\varepsilon(P) = U(P) - u(P)$  by definition, (II.23) can be used to establish the following equalities

$$\begin{aligned} \Delta_h \varepsilon(x) &= \Delta_h [U(P) - u(P)] \\ &= \Delta_h U(P) - \Delta_h u(P) \\ &= F(P) - \Delta_h u(P) \\ &= \Delta u(P) - \Delta_h u(P). \end{aligned}$$

Thus the error can be written as

$$\varepsilon(P) = h^2 \sum_{Q \in \Omega_h} G_h(P, Q) [\Delta_h u(Q) - \Delta u(Q)].$$

Taking the absolute value and employing the triangle inequality, we have

$$|\varepsilon(P)| \leq h^2 \sum_{Q \in \Omega_h} \left| G_h(P, Q) \right| \left| \Delta_h u(Q) - \Delta u(Q) \right|,$$

which is the desired result. □

Note that an upper bound for  $|\Delta_h u(Q) - \Delta u(Q)|$  is known for uniform and non-uniform discretizations by inequalities (II.4) and (II.6) respectively. The remaining lemmas go to establish upper and lower bounds on  $G_h(P, Q)$ .

**Lemma 4.** For  $P \in \bar{\Omega}_h$ ,

$$G_h(P, Q) \geq 0, \quad \forall Q \in \bar{\Omega}_h. \quad (\text{II.14})$$

*Proof.* Let  $Q \in \partial\Omega_h$ . If  $P = Q$ , then  $G_h(P, Q) = 1$ . When  $P \neq Q$ , then  $G_h(P, Q) = 0$ . Thus  $G_h(P, Q) \geq 0, \forall Q \in \partial\Omega_h$ .

Now let  $Q \in \Omega_h$ . We know that  $\Delta_h[-G_h(P, Q)] \geq 0 \forall Q \in \Omega_h$  by definition of Green's function. By the maximum principle,  $-G_h(P, Q)$  takes its maximum on the boundary implying that  $G_h(P, Q)$  takes its minimum on the boundary. But since  $G_h(P, Q) \geq 0$  on the boundary, it must be that  $G_h(P, Q) \geq 0, \forall Q \in \bar{\Omega}_h$ .  $\square$

**Lemma 5.** Let  $d_0$  be the diameter of the smallest circle circumscribing  $\bar{\Omega}_h$ , then

$$h^2 \sum_{Q \in \Omega_h} G_h(P, Q) \leq \frac{d_0^2}{16}, \quad \forall P \in \bar{\Omega}_h \quad (\text{II.15})$$

*Proof.* Let  $O$  be the center of the smallest circumscribed circle containing  $\bar{\Omega}_h$  with radius  $R$ . Define  $W(P) = \frac{r(P)^2}{4}$  where  $r$  is the Euclidean distance from  $o$  to  $P$  in the cartesian plane. Applying the discrete operator (II.5) to  $W(P)$  for  $P \in \bar{\Omega}_h$  we have

$$\begin{aligned} \Delta_h W(x, y) &= \frac{1}{2h^2} \left\{ \frac{r(x+eh, y)^2}{e(e+w)} + \frac{r(x-wh, y)^2}{w(e+w)} + \frac{r(x, y+nh)^2}{n(n+s)} \right. \\ &\quad \left. + \frac{r(x, y-sh)^2}{s(n+s)} - r(x, y)^2 \left( \frac{1}{ew} + \frac{1}{ns} \right) \right\} \\ &= \frac{1}{2h^2} \left\{ \frac{x^2 + 2eh + e^2h^2 + y^2}{e(e+w)} + \frac{x^2 - 2wh + w^2h^2 + y^2}{w(e+w)} \right. \\ &\quad \left. + \frac{x^2 + y^2 + 2nh + n^2h^2}{n(n+s)} + \frac{x^2 + y^2 - 2sh + s^2h^2}{s(n+s)} - \frac{x^2 + y^2}{ew} - \frac{x^2 + y^2}{ns} \right\} \\ &= \frac{1}{2h^2} \left\{ \frac{wx^2 + 2ewh + we^2h^2 + wy^2 + ex^2 - 2ewh + ew^2h^2 + ey^2}{ew(e+w)} \right. \\ &\quad \left. + \frac{sx^2 + sy^2 + 2nsh + sn^2h^2 + nx^2 + ny^2 - 2nsh + ns^2h^2}{ns(n+s)} \right. \\ &\quad \left. - \frac{x^2 + y^2}{ew} - \frac{x^2 + y^2}{ns} \right\} \end{aligned}$$

$$\begin{aligned}
&= \frac{1}{2h^2} \left\{ \frac{(e+w)x^2 + (e+w)y^2 + (e+w)ewh^2}{ew(e+w)} \right. \\
&\quad \left. + \frac{(n+s)x^2 + (n+s)y^2 + (n+s)nsh^2}{ns(n+s)} - \frac{x^2+y^2}{ew} - \frac{x^2+y^2}{ns} \right\} \\
&= \frac{1}{2h^2} \left\{ \frac{x^2+y^2+ewh^2}{ew} + \frac{x^2+y^2+nsh^2}{ns} - \frac{x^2+y^2}{ew} - \frac{x^2+y^2}{ns} \right\} \\
&= \frac{1}{2h^2} \left\{ \frac{ewh^2}{ew} + \frac{nsh^2}{ns} \right\}
\end{aligned}$$

The above equality simplifies to  $\Delta_h W(P) = 1$  for  $P \in \bar{\Omega}_h$ . We now define another mesh function

$$V(P) = h^2 \sum_{Q \in \Omega_h} G_h(P, Q)$$

By the definition of Green's function (II.9), we know that

$$\begin{aligned}
\Delta_h V(P) &= -1, \quad P \in \Omega_h \\
V(P) &= 0, \quad P \in \partial\Omega_h.
\end{aligned}$$

Since  $V(P) = 0$  when  $P \in \partial\Omega_h$ , then clearly  $W(P) + V(P) \leq \frac{D^2}{16}$  for  $P \in \partial\Omega_h$ . When  $P \in \Omega_h$ , we have  $\Delta_h W(P) + \Delta_h V(P) = \Delta_h [W(P) + V(P)] = 0$  implying that both minimum and maximum of sum of  $W(P) + V(P)$  occurs on the boundary by Lemma 1. Thus  $W(P) + V(P) \leq \frac{D^2}{16} \forall P \in \bar{\Omega}_h$ . It is also true that  $W(P) \geq 0$  everywhere such that  $V(P) \leq W(P) + V(P)$  concluding the proof.  $\square$

For the following lemmas, we introduce a partition of  $\Omega_h$  to distinguish between nodes with neighbors that are equidistant and those without. We define the sets as follows:

$$\begin{aligned}
R_h &= \{ P \in \Omega_h \mid e = w \text{ and } n = s \} \\
R_h^* &= \{ P \in \Omega_h \mid e \neq w \text{ or } n \neq s \}.
\end{aligned}$$

Notice that  $\Omega_h = R_h \cup R_h^*$ . We would like to further refine  $R_h^*$  into two additional subsets. Let  $N(P) = \{Q \in \bar{\Omega}_h \mid Q \text{ is adjacent to } P\}$ . Thus  $N(P)$  is the set of  $P$ 's neighbors and

consists of adjacent nodes whose function values appear in the discrete operator applied to point  $P$ . Define

$$\begin{aligned} A_h^* &= \{ P \in R_h^* \mid N(P) \subseteq \Omega_h \} \\ C_h^* &= \{ P \in R_h^* \mid N(P) \not\subseteq \Omega_h \}. \end{aligned}$$

Bramble and Hubbard assumed that all non-uniform nodes belonged to  $C_h^*$  and that  $A_h^* = \emptyset$ . The sets  $A_h^*$  and  $C_h^*$  are composed of interior non-uniformities and boundary adjacent non-uniformities respectively.

**Lemma 6.** For any  $P \in \bar{\Omega}_h$ ,

$$\sum_{Q \in C_h^*} G_h(P, Q) \leq 1. \quad (\text{II.16})$$

*Proof.* We begin by defining the mesh function  $W(P)$  given by

$$W(P) = \begin{cases} 1, & P \in \Omega_h \\ 0, & P \in \partial\Omega_h. \end{cases}$$

By Lemma 2, we may rewrite  $W(P)$  as

$$W(P) = h^2 \sum_{Q \in \Omega_h} G_h(P, Q)[- \Delta_h W(Q)] + \sum_{Q \in \partial\Omega_h} G_h(P, Q)W(Q).$$

If  $P \in \partial\Omega_h$ , the inequality is trivially satisfied by the definition of  $G_h(P, Q)$ . If  $P \in \Omega_h$ , the second summation equals zero. Since  $\Omega_h = R_h \cup A_h^* \cup C_h^*$ , we express the mesh function as

$$\begin{aligned} 1 &= h^2 \sum_{Q \in R_h} G_h(P, Q)[- \Delta_h W(Q)] \\ &+ h^2 \sum_{Q \in A_h^*} G_h(P, Q)[- \Delta_h W(Q)] + h^2 \sum_{Q \in C_h^*} G_h(P, Q)[- \Delta_h W(Q)]. \end{aligned} \quad (\text{II.17})$$

We now show that the first and second summations equal zero. Since the uniform discrete operator is a special case of the non-uniform operator, i.e. when  $e = w = n = s = 1$ , it

suffices to show that the second summation equals zero. Letting  $Q \in A_h^*$ , we have

$$\begin{aligned} -\Delta_h W(Q) &= -\frac{2}{h^2} \left\{ \frac{1}{e(e+w)} + \frac{1}{w(e+w)} + \frac{1}{n(n+s)} + \frac{1}{s(n+s)} - \left( \frac{1}{ew} + \frac{1}{ns} \right) \right\} \\ &= -\frac{2}{h^2} \left\{ \frac{w+e-(e+w)}{ew(e+w)} + \frac{s+n-(n+s)}{ns(n+s)} \right\} = 0. \end{aligned}$$

Since  $-\Delta_h W(Q) = 0$  for  $Q \in A_h^* \cup R_h$ , then

$$h^2 \sum_{Q \in A_h^*} G_h(P, Q) [-\Delta_h W(Q)] = h^2 \sum_{Q \in R_h} G_h(P, Q) [-\Delta_h W(Q)] = 0.$$

Hence, (II.17) reduces to

$$1 = h^2 \sum_{Q \in C_h^*} G_h(P, Q) [-\Delta_h W(Q)].$$

Applying the discrete operator to  $Q \in C_h^*$ , we have that

$$\begin{aligned} -\Delta_h W(Q) &= \frac{2}{h^2} \left\{ \frac{(e+w)W_0 - wW_e - eW_w}{ew(e+w)} + \frac{(n+s)W_0 - sW_n - nW_s}{ns(n+s)} \right\} \\ &= \frac{2}{h^2} \left\{ \frac{W_0 - W_e}{e(e+w)} + \frac{W_0 - W_w}{w(e+w)} + \frac{W_0 - W_n}{n(n+s)} + \frac{W_0 - W_s}{s(n+s)} \right\} \end{aligned}$$

Since  $W_0 = 1$  and at least one of the functions values  $W_e, W_w, W_n,$  or  $W_s$  equals zero, then the expression is greater than zero. Letting  $a = \max\{e, w, n, s\}$  we have that

$$\begin{aligned} -\Delta_h W(Q) &\geq \frac{2}{h^2} \left\{ \frac{W_0 - W_e}{2a^2} + \frac{W_0 - W_w}{2a^2} + \frac{W_0 - W_n}{2a^2} + \frac{W_0 - W_s}{2a^2} \right\} \\ &= \frac{1}{a^2 h^2} (4W_0 - W_e - W_w - W_n - W_s). \end{aligned}$$

Since  $a \leq 1$ , and  $(4W_0 - W_e - W_w - W_n - W_s) \geq 1$ , then  $-\Delta_h W(Q) \geq \frac{1}{h^2}$  leaving us with  $-h^2 \Delta_h W(Q) \geq 1$ . Since  $G_h(P, Q) \geq 0, \forall Q \in \bar{\Omega}_h$ , by Lemma 4, we can establish the inequalities

$$0 \leq \sum_{Q \in C_h^*} G_h(P, Q) * [1] \leq \sum_{Q \in C_h^*} G_h(P, Q) * [-h^2 \Delta_h W(Q)].$$

Since the far right expression equals 1 by definition of the mesh function representation of Lemma 2, then

$$\sum_{Q \in \mathcal{C}_h^*} G_h(P, Q) \leq 1, \quad \forall P \in \bar{\Omega}_h.$$

□

The above lemmas provide the foundation for Bramble and Hubbard's proof for domains with boundary adjacent non-uniformities. It should be mentioned that the mesh function defined in Lemma 6 is convex at non-uniform nodes and nowhere else. Their identification of a mesh function convex only at non-uniformities such that  $\frac{1}{h^2} \leq -\Delta_h W(Q)$  allows for establishment of an upper bound on the error contribution from boundary adjacent non-uniformities.

When non-uniformities are extended to the interior, it is easy to find functions that are convex only at non-uniformities. On the other hand, finding a function satisfying the property that  $\frac{1}{h^2} \leq -\Delta_h W(Q)$ ,  $\forall Q \in R_h^*$  and  $-\Delta_h W(Q) = 0$ ,  $\forall Q \in R_h$ , was far from trivial. Indeed, we failed to devise such a function and had to settle for a slightly weaker result that  $\frac{1}{h} \leq -\Delta_h W(Q)$ ,  $\forall Q \in R_h^*$  and zero in  $R_h$ . The following section details one such function and allows us to establish an upper bound on the error due to interior non-uniformities.

### II.3 New Mesh Function and Inequality for $R_h^*$

We begin this section by defining several new sets. We then introduce a mesh function  $Z(P)$  that has the properties that  $-\Delta_h Z(P) \geq \frac{1}{h}$ ,  $\forall P \in A_h^*$  and  $-\Delta_h Z(P) = 0$ ,  $\forall P \in R_h$ . Equipped with such a mesh function, we then establish an inequality allowing us to prove our final result.

Begin by considering the domain  $\bar{\Omega}_h$ . Let the coordinates  $(x_{\min}, y_{\min})$ ,  $(x_{\max}, y_{\min})$ ,  $(x_{\min}, y_{\max})$ , and  $(x_{\max}, y_{\max})$  be the corners of the smallest rectangle that contains  $\bar{\Omega}_h$ . Let  $d_x = x_{\max} - x_{\min}$  and  $d_y = y_{\max} - y_{\min}$ . We define two new sets as

$$X = \{ x_i \mid x_{\min} < x_i < x_{\max} \text{ and } (x_i, y_k) \in A_h^* \},$$

$$Y = \{ y_i \mid y_{\min} < y_i < y_{\max} \text{ and } (x_k, y_i) \in A_h^* \}.$$

Taking note of the cardinality of  $X$  and  $Y$ , we set  $O_X = |X|$  and  $O_Y = |Y|$ . We define new sets as the union of  $X$  and  $Y$  and their minimum and maximum boundary values in each direction given by

$$\begin{aligned} X^* &= X \cup \{x_{\min}, x_{\max}\} = \{x_0^*, x_1^*, \dots, x_{O_X}^*, x_{O_X+1}^*\} \\ Y^* &= Y \cup \{y_{\min}, y_{\max}\} = \{y_0^*, y_1^*, \dots, y_{O_Y}^*, y_{O_Y+1}^*\} \end{aligned}$$

where  $x_i^*$  for  $i = \{1, 2, \dots, O_X + 1\}$  and  $y_j^*$  for  $j = \{1, 2, \dots, O_Y + 1\}$  denote elements of  $X^*$  and  $Y^*$  respectively. We order the elements of  $X^*$  and  $Y^*$  such that  $x_{i-1}^* < x_i^* < x_{i+1}^*$  and  $y_{j-1}^* < y_j^* < y_{j+1}^*$ . Note that  $x_0^* = x_{\min}$ ,  $y_0^* = y_{\min}$ ,  $x_{O_X+1}^* = x_{\max}$ , and  $y_{O_Y+1}^* = y_{\max}$ . Finally, we make use of the sets  $X^*$  and  $Y^*$  by introducing sub-domains of  $\Omega_h$ . Define

$$D_{l,m} = \{ (x, y) \in \bar{\Omega}_h \mid x_{l-1}^* \leq x \leq x_l^* \text{ and } y_{m-1}^* \leq y \leq y_m^* \},$$

for  $0 < l \leq O_X + 1$  and  $0 < m \leq O_Y + 1$ .

Thus, each sub-domain is bounded by successive mesh non-uniformities in the  $x$  and  $y$  directions or the boundary,  $\partial\Omega_h$ . Note that these sub-domains will have non-empty intersections when interior non-uniformities are present. Define

$$\begin{aligned} D &= \{P \in (\Omega_h \cap \text{interior}(D_{l,m})) \mid \text{for any } 0 < l \leq O_X + 1 \text{ and } 0 < m \leq O_Y + 1\}, \\ \partial D &= \{P \in (\Omega_h \cap D_{l,m} \cap D_{r,s}) \mid l \neq r \text{ or } m \neq s\}. \end{aligned}$$

Note that  $\partial D$  is the set of interior nodes where a non-uniformity exists. Thus, we can write  $A_h^* \subseteq \partial D$  and  $\Omega_h = D \cup \partial D$ . We are now ready to define our local mesh function which is given by

$$z_{l,m}(x, y) = \frac{x}{l} + \frac{y}{m} + a_l + b_m, \quad \text{for } (x, y) \in D_{l,m}, \quad (\text{II.18})$$

with  $a_l$  and  $b_m$  defined as

$$a_l = a_0 + \sum_{k=1}^{l-1} \frac{x_k^*}{k(k+1)}, \quad b_m = b_0 + \sum_{k=1}^{m-1} \frac{y_k^*}{k(k+1)}, \quad (\text{II.19})$$

where  $a_0$  and  $b_0$  are chosen such that  $z_{1,m}(x_0^*, y) = \frac{y}{m} + b_m$  and  $z_{l,1}(x, y_0^*) = \frac{x}{l} + a_l$ . For notational simplicity, we let  $c_{l,m} = a_l + b_m$  when appropriate. Globally, we define

$$Z(x, y) \Big|_{l,m} = z_{l,m}(x, y), \quad \forall (x, y) \in \bar{\Omega}_h. \quad (\text{II.20})$$

Figure II.2 shows an example of the mesh function  $Z(x, y)$ .

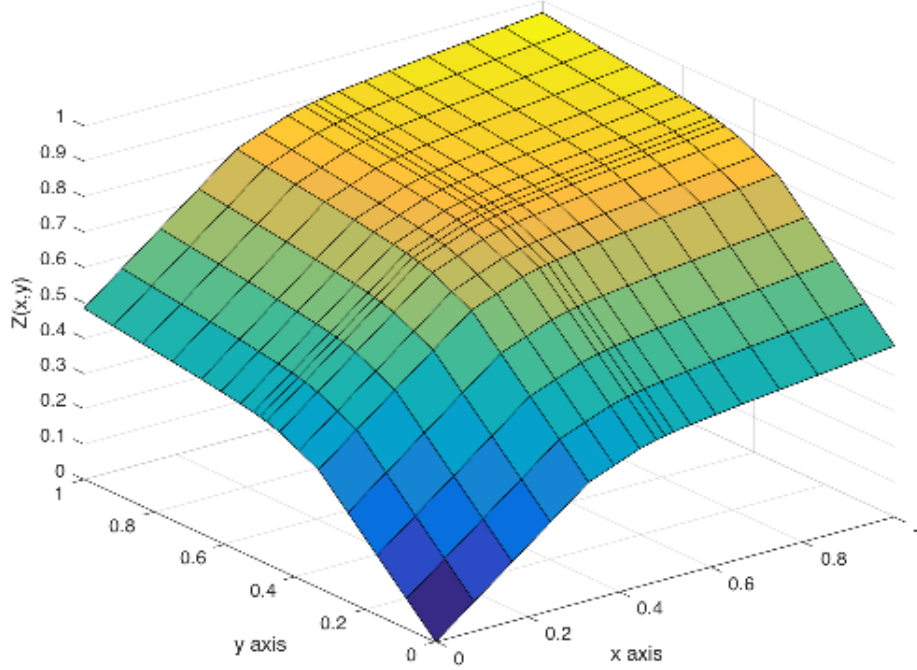


Figure II.2: Example of the mesh function  $Z(x, y)$

It can be seen that  $Z(x, y)$  is a collection of piecewise planes over the domain. Note that the normal vector of the surface only changes after crossing non-uniform grid-lines. A one-dimensional cross-section in the  $xz$ -plane is shown in Figure II.3 with asterisks above the curve indicating locations at which the slope changes.

**Lemma 7.** *The piecewise linear mesh function  $Z(P)$  is globally continuous over  $\Omega_h$ .*

*Proof.* Rather than relying on Figure II.2 as proof, we provide a mathematical argument. When  $P \notin \partial D$ , then  $Z(P)$  is a linear function and therefore continuous. When  $P \in \partial D$ , then without loss of generality,  $P \in (D_{l,m} \cap D_{l+1,m+1})$  for some  $l, m$ . Further,  $P = (x_l^*, y_m^*)$

for  $x_l^* \in X^*$  and  $y_m^* \in Y^*$ . By the definition of  $Z(P)$  we have

$$\begin{aligned}
Z(x_l^*, y_m^*) \Big|_{l,m} &= \frac{x_l^*}{l} + \frac{y_m^*}{m} + a_0 + \sum_{k=1}^{l-1} \frac{x_k^*}{k(k+1)} + b_0 + \sum_{k=1}^{m-1} \frac{y_k^*}{k(k+1)} \\
&= \frac{(l+1)x_l^*}{l(l+1)} + \frac{(m+1)y_m^*}{m(m+1)} + a_0 + \sum_{k=1}^{l-1} \frac{x_k^*}{k(k+1)} + b_0 + \sum_{k=1}^{m-1} \frac{y_k^*}{k(k+1)} \\
&= \frac{x_l^*}{l+1} + \frac{y_m^*}{m+1} + a_0 + \frac{x_l^*}{l(l+1)} + \sum_{k=1}^{l-1} \frac{x_k^*}{k(k+1)} + b_0 + \frac{y_m^*}{m(m+1)} + \sum_{k=1}^{m-1} \frac{y_k^*}{k(k+1)} \\
&= \frac{x_l^*}{l+1} + \frac{y_m^*}{m+1} + a_0 + \sum_{k=1}^l \frac{x_k^*}{k(k+1)} + b_0 + \sum_{k=1}^m \frac{y_k^*}{k(k+1)} \\
&= Z(x_l^*, y_m^*) \Big|_{l+1, m+1}.
\end{aligned}$$

Since  $Z(P)$  is continuous for all  $P \in D$  and  $Z(x_l^*, y_m^*) \Big|_{l,m} = Z(x_l^*, y_m^*) \Big|_{l+1, m+1}$  for all  $P \in \partial D$ , then  $Z(P)$  is continuous for all  $P \in \Omega_h$ .  $\square$

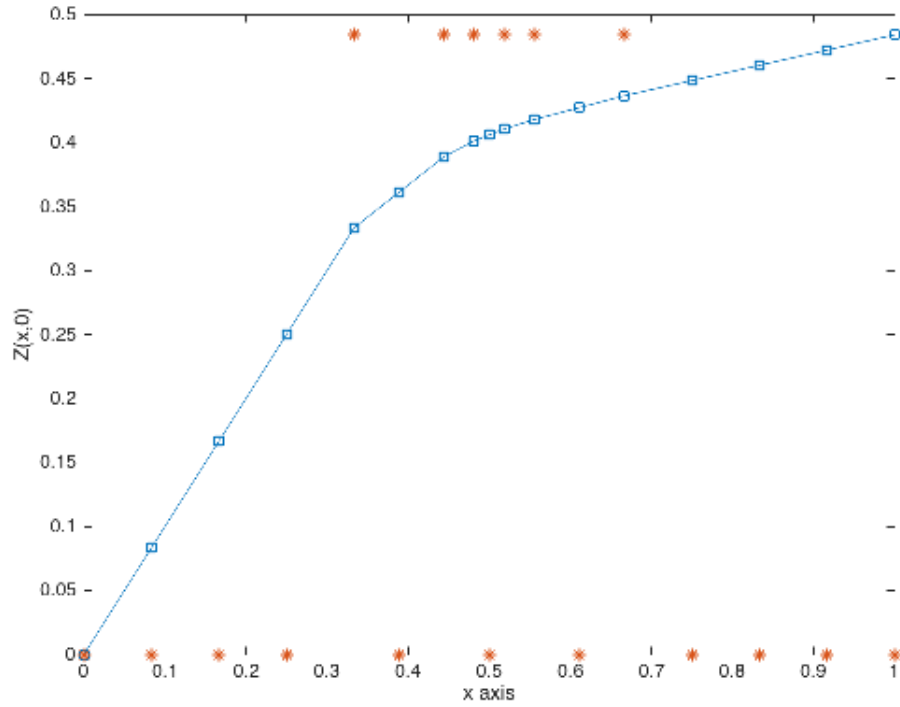


Figure II.3: Plot of  $x$  vs.  $Z(x, 0)$

**Lemma 8.** For mesh function  $Z(Q)$ ,

$$-\Delta_h Z(Q) = 0 \quad \forall Q \in D.$$

*Proof.* Let  $Q \in D$ . Then  $Q \in \text{interior}(D_{l,m})$  for some  $l$  and  $m$ . Therefore the slope and intercept of  $Z(P)$  is the same at all of  $Q$ 's neighbors. Applying the discrete operator to  $Z(Q)$  we have

$$\begin{aligned} \Delta_h Z(Q) = & \frac{2}{h^2 ew(e+w)} \left\{ \frac{w(x+eh)}{l} + \frac{wy}{m} + wc_{l,m} + \frac{e(x-wh)}{l} + \frac{ey}{m} + ec_{l,m} \right. \\ & \left. - \left( \frac{wx}{l} + \frac{wy}{m} + ec_{l,m} \right) - \left( \frac{ex}{l} + \frac{ey}{m} + ec_{l,m} \right) \right\} \\ & + \frac{2}{h^2 ns(n+s)} \left\{ \frac{sx}{l} + \frac{s(y+nh)}{m} + sc_{l,m} + \frac{nx}{l} + \frac{n(y-sh)y}{m} + nc_{l,m} \right. \\ & \left. - \left( \frac{sx}{l} + \frac{sy}{m} + sc_{l,m} \right) - \left( \frac{nx}{l} + \frac{ny}{m} + nc_{l,m} \right) \right\}. \end{aligned}$$

Since  $e = w$  and  $n = s$ , it is easy to show through algebraic manipulation that all terms cancel. Therefore  $-\Delta_h Z(Q) = 0, \forall Q \in D$ . □

**Lemma 9.** For the mesh function  $Z(Q)$ ,

$$-\Delta_h Z(Q) \geq \frac{1}{h} \left\{ \frac{1}{O_X^2 + O_X} + \frac{1}{O_Y^2 + O_Y} \right\} \quad \forall Q \in \partial D.$$

*Proof.* We begin by letting  $Q \in \partial D$  which implies that an interior non-uniformity in the mesh exists. Using Figure II.2 as a guide, we focus our attention on nodes where the plane equation changes. Without loss of generality, let  $Q = (x^*, y^*)$  where  $x^* \in X^*$  and  $y^* \in Y^*$ . Applying the discrete operator to  $Q$  gives

$$\begin{aligned} \Delta_h Z(x^*, y^*) = & \frac{2}{h^2} \left\{ \frac{(x^* + eh)/(l+1) + y^*/m + a_{l+1} + b_m}{e(e+w)} \right. \\ & + \frac{(x^* - wh)/l + y^*/m + a_l + b_m}{w(e+w)} + \frac{x^*/l + (y^* + nh)/(m+1) + a_l + b_{m+1}}{n(n+s)} \\ & \left. + \frac{x^*/l + (y^* - sh)/m + a_l + b_m}{s(n+s)} + \left( \frac{1}{ew} + \frac{1}{ns} \right) \frac{x^*}{l} + \frac{y^*}{m} + a_l + b_m \right\}. \end{aligned}$$

Through the use of Lemma 7 and extensive algebraic simplification, it can be shown that

$$-\Delta_h Z(Q) = \frac{2}{h} \left\{ \frac{1}{(l^2 + l)(e + w)} + \frac{1}{(m^2 + m)(n + s)} \right\}.$$

Since  $e, w, n, s \leq 1$ , then

$$-\Delta_h Z(Q) \geq \frac{1}{h} \left\{ \frac{1}{l^2 + l} + \frac{1}{m^2 + m} \right\}.$$

The right hand side of the inequality will shrink as  $l$  and  $m$  grow. Since  $l$  and  $m$  will take their maximum values at the interface between  $D_{O_X, O_Y}$  and

$D_{(O_X+1), (O_Y+1)}$ , then

$$-\Delta_h Z(Q) \geq \frac{1}{h} \left\{ \frac{1}{O_X^2 + O_X} + \frac{1}{O_Y^2 + O_Y} \right\}, \quad \forall Q \in \partial D,$$

thus concluding the proof. □

**Lemma 10.** For mesh function  $Z(Q)$ ,

$$Z(Q) \leq d_x + d_y, \quad \forall Q \in \bar{\Omega}_h,$$

where  $d_x$  and  $d_y$  are the lengths of the smallest rectangle containing  $\bar{\Omega}_h$  in the  $x$  and  $y$  directions respectively.

*Proof.* It is easily seen by the definition of  $Z(P)$  that as  $O_X$  and  $O_Y$  grow, the maximum value of  $Z(P)$  shrinks. Thus, given some continuous domain  $\bar{\Omega}$ , the maximum possible value of  $Z(P)$  will occur when there are no interior non-uniformities in the discretized domain  $\Omega_h$ . Suppose that  $X = Y = \emptyset$ . Then  $D_{1,1} \cap \Omega_h = \Omega_h$  and  $\partial D_{1,1} \cap \partial \Omega_h = \partial \Omega_h$ . Thus it is true that  $Z(x, y) = x + y + a_0 + b_0$ ,  $\forall (x, y) \in \bar{\Omega}_h$ . Since  $a_0$  and  $b_0$  are defined such that  $Z(x_{min}, y_{min}) = 0$ , then  $Z(x_{max}, y_{max}) = d_x + d_y$ . Since  $x \leq x_{max}$  and  $y \leq y_{max}$  for all  $(x, y) \in \bar{\Omega}_h$ , then

$$Z(P) \leq d_x + d_y, \quad \forall P \in \bar{\Omega}_h.$$

□

**Theorem 1.** For any  $P \in \Omega_h$ ,

$$\sum_{Q \in \partial D} G_h(P, Q) \leq \frac{d_x + d_y}{h\{(O_X^2 + O_X)^{-1} + (O_Y^2 + O_Y)^{-1}\}}. \quad (\text{II.21})$$

*Proof.* Let  $P \in \Omega_h$ . If  $\partial D = \emptyset$ , the inequality is vacuously true. Thus assume that  $\partial D \neq \emptyset$ .

We begin by noting the  $\bar{\Omega}_h = D \cup \partial D \cup \partial\Omega_h$ . Using Lemma 2, we can rewrite  $Z(P)$  as

$$Z(P) = h^2 \sum_{Q \in D \cup \partial D} G_h(P, Q)[- \Delta_h Z(Q)] + \sum_{Q \in \partial\Omega_h} G_h(P, Q)Z(Q).$$

Since  $P \in \Omega_h$ , then the second summation drops and we can rewrite as

$$Z(P) = h^2 \sum_{Q \in D} G_h(P, Q)[- \Delta_h Z(Q)] + h^2 \sum_{Q \in \partial D} G_h(P, Q)[- \Delta_h Z(Q)].$$

By Lemma 8, the summation over  $D$  equals zero, hence

$$Z(P) = h^2 \sum_{Q \in \partial D} G_h(P, Q)[- \Delta_h Z(Q)].$$

By Lemmas 9 and 10, we know

$$d_x + d_y \geq h \sum_{Q \in \partial D} G_h(P, Q)[(O_X^2 + O_X)^{-1} + (O_Y^2 + O_Y)^{-1}].$$

Since  $O_X \geq 0$ ,  $O_Y \geq 0$  and  $h > 0$ , then dividing through by  $h[(O_X^2 + O_X)^{-1} + (O_Y^2 + O_Y)^{-1}]$  yields the result.  $\square$

We are now equipped with the necessary foundation to prove the main result.

#### II.4 Error over General Domain with Non-Uniform Interior Mesh

In this section, we provide an error bound for a non-uniform mesh throughout the interior of a general domain. Furthermore, the resulting inequality provides proof that the order of convergence remains 2 with non-uniformity extended through the interior of the domain. This result contrasts the naive error which suggests that the order of convergence for a non-uniform mesh is 1.

**Theorem 2.** Let  $u(P)$  be a solution to (II.1) and  $U(P)$  be the solution to (II.23). Then the error,  $\varepsilon(P) = u(P) - U(P)$ , satisfies the inequality

$$|\varepsilon(P)| \leq \frac{2h^2}{3} \left\{ \frac{d_0^2 M_4}{64} + M_3 \left[ h + \frac{d_x + d_y}{(O_X^2 + O_x)^{-1} + (O_Y^2 + O_Y)^{-1}} \right] \right\}, \quad (\text{II.22})$$

where

- $d_0$ : diameter of smallest circle containing  $\bar{\Omega}_h$ ,
- $d_x, d_y$ : width and height respectively of the smallest rectangle containing  $\bar{\Omega}_h$ ,
- $M_3, M_4$ : maximum magnitude of third and fourth derivatives of the function respectively,
- $O_X, O_Y$ : number of non-boundary adjacent non-uniformities in  $x$  and  $y$  directions respectively,
- $h$ : largest step-size of  $\Omega_h$ .

*Proof.* Let  $u(P)$  be a solution to (II.1) and  $U(P)$  be the solution to (II.23). By Lemma 3,

$$|\varepsilon(P)| \leq h^2 \sum_{Q \in \Omega_h} \left| G_h(P, Q) \right| \left| \Delta_h u(Q) - \Delta u(Q) \right|.$$

Note that  $\Omega_h = R_h \cup R_h^* = R_h \cup A_h^* \cup C_h^*$ . By Lemma 4 which implies that  $|G_h(P, Q)| = G_h(P, Q)$ , we can split the summation and rewrite as

$$\begin{aligned} |\varepsilon(P)| \leq h^2 & \left\{ \sum_{Q \in R_h} G_h(P, Q) \left| \Delta u(Q) - \Delta_h u(Q) \right| \right. \\ & \left. + \sum_{Q \in A_h^*} G_h(P, Q) \left| \Delta u(Q) - \Delta_h u(Q) \right| + \sum_{Q \in C_h^*} G_h(P, Q) \left| \Delta u(Q) - \Delta_h u(Q) \right| \right\}. \end{aligned}$$

Noting that  $A_h^* \subseteq \partial D$ , the following inequality holds

$$\begin{aligned} |\varepsilon(P)| \leq h^2 & \left\{ \sum_{Q \in R_h} G_h(P, Q) \left| \Delta u(Q) - \Delta_h u(Q) \right| \right. \\ & \left. + \sum_{Q \in \partial D} G_h(P, Q) \left| \Delta u(Q) - \Delta_h u(Q) \right| + \sum_{Q \in C_h^*} G_h(P, Q) \left| \Delta u(Q) - \Delta_h u(Q) \right| \right\}. \end{aligned}$$

By inequalities (II.4) and (II.6), Lemmas 4, 5, and 6, and Theorem 1, we have

$$\begin{aligned} h^2 \sum_{Q \in R_h} G_h(P, Q) |\Delta u(Q) - \Delta_h u(Q)| &\leq \left(\frac{d_0^2}{16}\right) \left(\frac{h^2 M_4}{6}\right), \\ h^2 \sum_{Q \in \partial D} G_h(P, Q) |\Delta u(Q) - \Delta_h u(Q)| &\leq h^2 \left(\frac{d_x + d_y}{h[(O_x^2 + O_X)^{-1} + (O_Y^2 + O_Y)^{-1}]}\right) \left(\frac{2hM_3}{3}\right), \\ h^2 \sum_{Q \in C_h^*} G_h(P, Q) |\Delta u(Q) - \Delta_h u(Q)| &\leq h^2(1) \left(\frac{2hM_3}{3}\right). \end{aligned}$$

Rewriting, we are left with our main result

$$|\varepsilon(P)| \leq \frac{2h^2}{3} \left\{ \frac{d_0^2 M_4}{64} + M_3 \left[ h + \frac{d_x + d_y}{(O_x^2 + O_X)^{-1} + (O_Y^2 + O_Y)^{-1}} \right] \right\}.$$

□

Note that the error remains an  $O(h^2)$  approximation even with interior non-uniformities. The magnitude of error depends on the number of non-uniform nodes throughout the interior. The result implies that the order of convergence is two in contrast to the commonly accepted  $O(h)$  as the derivation of the Shortley-Weller equation suggests.

## II.5 Remarks Considering Growth of $O_X$ and $O_Y$

In the event  $O_X$  and  $O_Y$  are fixed initially, it is clear that a true  $O(h^2)$  approximation is obtained over a non-uniform mesh. Successive mesh refinements will place new grid-lines at the midpoints of existing nodes. On the other hand, the true power in Theorem 2 lies in the flexibility to study non-standard discretizations. One such refinement scheme is the graded adaptive mesh.

Our work was motivated by domains with a corner singularity. In particular, we sought to show that the SWE provides an  $O(h^2)$  approximation for the following system

$$\begin{cases} \Delta_h U(P) = -1, & P \in \Omega_h, \\ U(P) = 0, & P \in \partial\Omega_h, \end{cases} \quad (\text{II.23})$$

where  $\bar{\Omega}_h$  is the discretized version of the flag shaped domain given in (I.2) and the solution shown in Figure I.2. By using a graded mesh for successive refinements, we sought to tamp out the relative error growth at the reentrant corner without significantly increasing computational cost. With the motivating problem as our example, we would like to introduce a non-uniformity in the  $x$  and  $y$  direction adjacent to the interior corner.

For the coarsest mesh, we introduce two non-uniformities in both directions such that  $O_X = O_Y = 2$ . Suppose the initial maximum mesh spacing is given by  $h_0$ . For each refinement, we place new grid-lines at the midpoint of all nodes with the exception of points adjacent to the interior corner where the singularity is located. Suppose the distance from interior corner to the adjacent nodes is  $\delta$ . Then we place new grid-lines at  $\frac{\delta}{3}$  from the interior corner rather than  $\frac{\delta}{2}$ . Continuing on with successive mesh refinements in this fashion, yields the following table indicating the growth of  $O_X$ ,  $O_Y$  and the decay of  $h$ .

Table II.1: Growth of  $O_X$  and  $O_Y$

Refinement Level	Max step size	$O_X, O_Y$
1	$h_0$	2
2	$\frac{h_0}{2}$	4
3	$\frac{h_0}{4}$	6
4	$\frac{h_0}{8}$	8
5	$\frac{h_0}{16}$	10
$\vdots$	$\vdots$	$\vdots$
$n$	$\frac{h_0}{2^{n-1}}$	$2n$

Turning our attention to (II.22), we would like to ensure that the error does not grow. Thus, we investigate the behavior of the term

$$\frac{2M_3 h^2 (d_x + d_y)}{3[(O_X^2 + O_X)^{-1} + (O_Y^2 + O_Y)^{-1]}.$$

Since  $M_3$ ,  $d_x$ , and  $d_y$  are constant, we set  $\frac{2M_3(d_x+d_y)}{3} = 1$  for notational simplicity. Our expression reduces to

$$\frac{h^2}{(O_X^2 + O_X)^{-1} + (O_Y^2 + O_Y)^{-1}}.$$

Letting  $O = \max\{O_X, O_Y\}$ , then

$$\frac{h^2}{(O_X^2 + O_X)^{-1} + (O_Y^2 + O_Y)^{-1}} \leq \frac{h^2}{2} (O^2 + O).$$

Beginning with an initial max step size of  $h_0$ , then the  $n^{\text{th}}$  refinement expression will be given by

$$\frac{h_0^2}{2^{2n-1}} (4n^2 + 2n) = h_0^2 \left( \frac{n^2}{2^{2n-3}} + \frac{n}{2^{2n-2}} \right)$$

By L'Hopitals rule, we have that

$$\lim_{n \rightarrow \infty} h_0^2 \left( \frac{n^2}{2^{2n-3}} + \frac{n}{2^{2n-2}} \right) = \lim_{n \rightarrow \infty} h_0^2 \left( \frac{2n}{2^{2n-3}} + \frac{1}{2^{2n-2}} \right) = 0.$$

Thus our approximation when employing a graded adaptive mesh converges to the exact solution. Convergence to zero is not a strong result; this merely confirms what is expected. In the limiting case where the number of nodes goes to infinity, our approximation approaches the continuous case as required. Ongoing work involves determining the rate at which the non-uniform interior error term shrinks for different discretization schemes.

### III. NUMERICAL SOLUTIONS AND FAST SOLVERS

As outlined in Chapter I, the finite difference method discretizes the domain over which a differential equation (DE) is defined. A discrete operator is derived through a Taylor Series expansion that approximates the differential operator. This discrete operator can be expressed as a matrix,  $A$ , and the DE can be recast as a system of linear equations. These equations are then solved to determine approximate solution values at nodal locations. For illustrative purposes, consider the following boundary value problem in one-dimension

$$\begin{cases} \Delta u(x) = f(x), & \text{for } x \in (0, 1), \\ u(x) = 0, & \text{at } x = 0, 1. \end{cases} \quad (\text{III.1})$$

We discretize the unit interval uniformly with  $N$  nodes. Thus, the step-size is given by  $h = \frac{1}{N-1}$ . The discretized domain is then the set of points

$$\bar{\Omega}_h = \{0, h, 2h, \dots, (N-2)h, 1\} = \{x_1, x_2, \dots, x_N\}.$$

Let  $u_i$  and  $f_i$  be the corresponding solution and force function values at  $x_i$  respectively. The difference equation is given by

$$\Delta_h u_i = \frac{u_{i-1} - 2u_i + u_{i+1}}{h^2} = f_i.$$

It can be seen that the above difference equation gives rise to the system of linear equations

$$A\vec{u} = \vec{b}, \quad (\text{III.2})$$

where

$$A = \frac{1}{h^2} \begin{bmatrix} -2 & 1 & 0 & 0 & 0 & \dots & 0 \\ 1 & -2 & 1 & 0 & 0 & \dots & 0 \\ 0 & 1 & -2 & 1 & 0 & \dots & 0 \\ 0 & 0 & 1 & -2 & 1 & \dots & 0 \\ 0 & 0 & 0 & 1 & -2 & \dots & 0 \\ \vdots & \vdots & \vdots & \vdots & \vdots & \ddots & \vdots \\ 0 & 0 & 0 & 0 & 0 & 1 & -2 \end{bmatrix}, \quad \vec{u} = \begin{bmatrix} u_2 \\ u_3 \\ u_4 \\ u_5 \\ u_6 \\ \vdots \\ u_{N-1} \end{bmatrix}, \quad \vec{f} = \begin{bmatrix} f_2 \\ f_3 \\ f_4 \\ f_5 \\ f_6 \\ \vdots \\ f_{N-1} \end{bmatrix}.$$

Equations for  $x_1$  and  $x_N$  are omitted since the solution's value is known by boundary conditions (BC). In the case of non-zero BC, they would be added to right side for all equations of boundary adjacent nodes.

### III.1 Basic Solvers

There are many methods for solving (III.2), the most obvious of which being the inversion of  $A$  such that  $\vec{u} = A^{-1}\vec{f}$ . Unfortunately, most scientific and engineering applications seek to solve systems of equations corresponding to a million unknowns. As is well known, Gaussian-elimination to invert an  $n \times n$  matrix costs  $O(n^3)$  floating-point operations (FLOPs). This prohibitive computational cost has kept mathematicians busy for the past century finding more efficient methods to invert matrices.

Rather than solving the system directly through matrix inversion, it is possible to use iterative methods. These methods can be characterized by guessing a solution then exploiting properties of the system matrix to converge on the exact solution. The most basic iterative solvers are known as relaxation methods and include Jacobi and Gauss-Seidel (GS) smoothing.

These smoothing techniques are guaranteed to converge provided the matrix is diagonally dominant, i.e. the sum of off diagonal entries in any row is less than or equal to the row's diagonal entry. It is problematic that such simplistic iterative methods converge slowly. GS smoothing quickly eliminates high frequency error, but fails to address global

error in a timely fashion. In other words, given a completely random guess of the solution vector, GS smoothing will quickly generate a smooth curve, but a smooth curve with a large residual. An example of this high frequency smoothing is shown in Figure III.1 for the boundary value problem (III.1) with  $f(x) = -\pi^2 \sin(\pi x)$ . The choppy blue curve is the initial solution guess. Every 25<sup>th</sup> iterate has been plotted on the same chart. Although the high frequency error is quickly eliminated, the smoother requires many iterations to converge to the exact solution which is the curve in heavy black. Over 20,000 smooths were required before the relative error,  $\|\vec{f} - A\vec{u}\|/\|\vec{f}\|$ , dropped below a tolerance of  $10^{-6}$ . The inability to correct global error makes GS smoothing a poor choice for most applications.

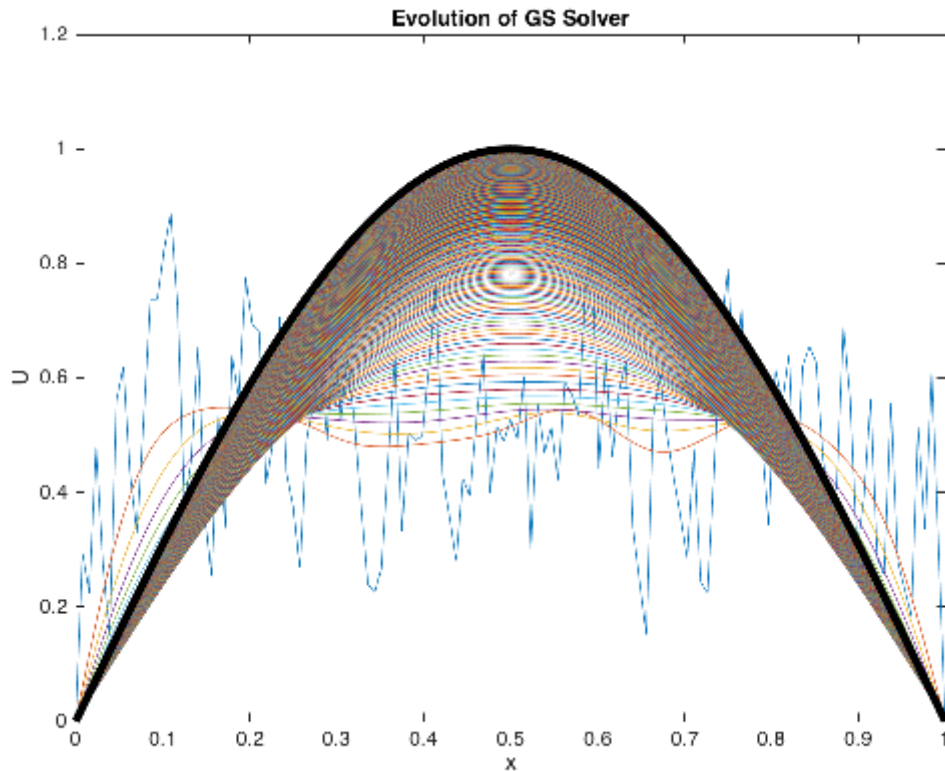


Figure III.1: Evolution of Gauss-Seidel smoothing: every 25<sup>th</sup> iterate plotted

### III.2 The Multigrid Method

It is for this reason that more efficient algorithms have been developed to quickly generate good initial guesses or accelerate the convergence of iterative solvers. There are a number of popular fast-solvers and pre-conditioners such as the generalized minimum residual method (GMRES), gradient descent, and the conjugate gradient method. This thesis focuses on the

Multigrid method (MG) which can generally obtain a solution in  $O(n)$  time; a considerable improvement from Gaussian elimination.

---

**Algorithm 1** Multigrid V-Cycle

---

Begin main routine

Construct system matrix:  $A$

Guess solution:  $u$

Set right side:  $f$

while (error > tolerance)

Smooth solution:  $u = \text{smoother}(u)$

Calculate residual:  $r = f - Au$

Calculate correction:  $c = \text{multiGridVcycle}(r)$

Correct solution:  $u = u + c$

Smooth solution:  $u = \text{smoother}(u)$

Calculate residual:  $r = f - Au$

Calculate error: error =  $\|r\|/\|f\|$

loop

End main routine

Function  $C_h = \text{multiGridVcycle}(r_h)$

Restrict  $r_h$  to coarser grid:  $r_H = \text{restrict}(r_h)$

if ( $r_H$  is restricted to coarsest grid) then

Solve for  $C_H$  exactly:  $C_H = A^{-1}r_H$

Else

Calculate residual's residual:  $R_H = r_H - AC_H$

Descend into V-Cycle:  $C_H = \text{multiGridVcycle}(R_H)$

end if

Prolong  $C_H$  to finer grid:  $C_h = \text{prolong}(C_H)$

Smooth  $C_h$ :  $C_h = \text{smoother}(C_h)$

Return  $C_h$

End function

---

The multigrid method takes advantage of a relaxation methods' ability to quickly smooth "high frequency error" by using a collection of meshes with varying step-sizes or resolutions. For a system with a single unknown, the global and high-frequency error are identical. Small systems can be solved directly or with a limited number of smooths. As more unknowns are introduced, there is a significant discrepancy between local and global error. The idea is to use an appropriate mesh that quickly smooths the error of each frequency allowing for rapid convergence. Algorithm 1 outlines the V-cycle MG (MGV) solver used for the majority of our computational work. The MGV solver uses a defined number of meshes at different resolutions and calculates a correction to the solution on each grid. These corrections are combined to give a more accurate "guess" for the next iteration in the

V-cycle. Figure III.2 shows the evolution of our MGV solution iterates for the same boundary value problem with all iterations plotted; only 18 were required.

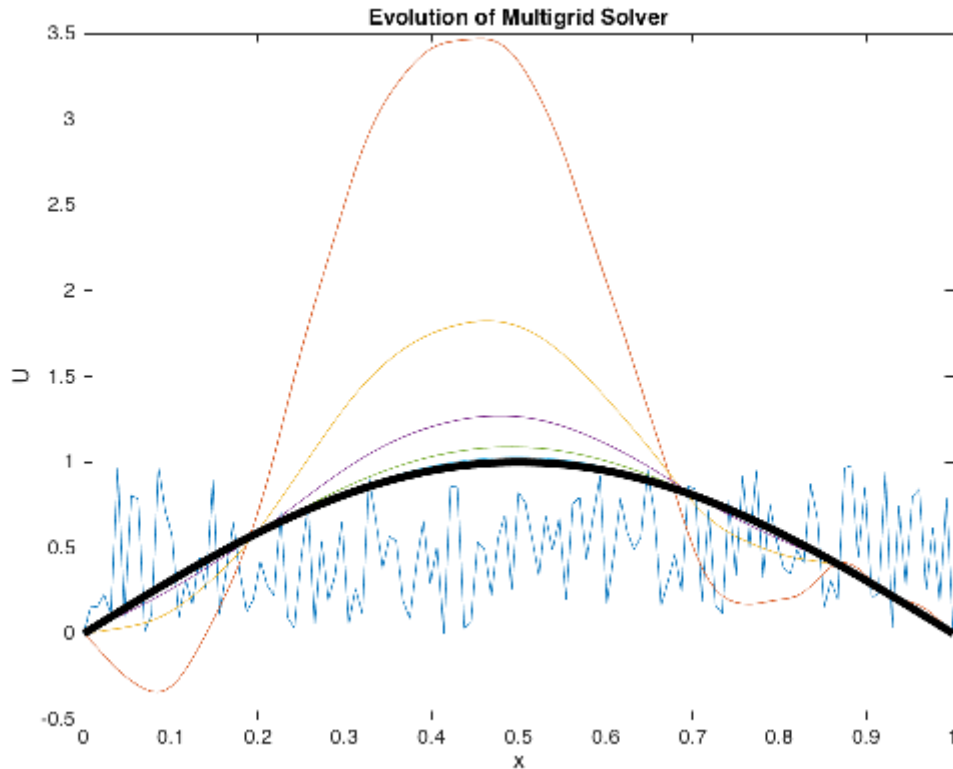


Figure III.2: Evolution of multigrid solver: every iterate plotted

Table III.1 shows the time to solution of MGV versus GS and MATLAB's built-in backslash operator. When solving systems with less than 30,000 unknowns, the backslash operator leads the pack. When system size becomes large, MGV takes a fraction of the time and shows why it is a popular choice in scientific computing. Its speed becomes more apparent in higher dimensions. For PDE's that evolve with time, this dramatic improvement in speed allows for simulations to be computed on laptops rather than super-computers.

A defining characteristic of MG is what is known as uniform convergence, i.e. regardless of the number of unknowns, an MG solver requires a fixed number of iterations through the V-cycle. In contrast, applying the GS smoother alone will require more smooths as the number of unknowns increases. This can be understood by considering how it smooths high-frequency error well but fails to handle global error efficiently. As the number of unknowns increase, high-frequency error becomes more localized.

Table III.1: Solution time in seconds for different methods

Level	Number of Unknowns	GS Smoother	Backslash Operator	Multi-Grid
10	1023	241.848852	0.021766	0.202236
11	2047	1551.401435	0.028834	0.241774
12	4095	11444.134741	0.049703	0.279627
13	8191	Too slow	0.115449	0.340790
14	16383	Too slow	0.385509	0.408269
15	32767	Too slow	1.643035	0.716387
16	65535	Too slow	9.436627	1.235823
17	131071	Too slow	51.876676	2.122150
18	262143	Too slow	227.718474	3.956959

### III.3 Limitations of the Multigrid Method for Graded Meshes

There is a problem though: the proof for uniform convergence of MG is contingent on symmetry of the system matrix. A motivation for this thesis was how to deal with the singular behavior of certain PDE's via non-uniform discretizations. By design, the resultant system matrix is non-symmetric. The goal of the numerical portion of this thesis was to develop an MG solver that exhibited uniform convergence.

Table III.2: Node placement for different  $\kappa$  values

$\kappa$	Node 1	Node 2	Node 3	Node 4	Node 5
1/2	0	1/4	2/4	3/4	1
1/3	0	2/6	3/6	4/6	1
1/4	0	3/8	4/8	5/8	1
1/5	0	4/10	5/10	6/10	1
1/10	0	9/20	10/20	11/20	1

This simple goal has proven elusive. For our analysis, we considered the boundary value problem (III.1) over a number of non-uniform discretizations. All discretizations differed by their system sizes and grading ratios. The grading ratio, given as  $\kappa$ , specifies how aggressively new nodes will be placed to the point of interest. Here,  $\kappa \in (0, 1/2]$  with smaller values indicating a more aggressive grading. In the standard case,  $\kappa = 1/2$  and gives a uniformly spaced mesh.

Table III.2 shows nodal location of a five-point graded mesh in one dimension with the point of interest at  $x = 1/2$  for different grading ratios. Fractions are left in reducible form to assist in pattern recognition. For successive mesh refinements, new nodes are placed at the midpoints of existing nodes everywhere except between the point of interest and its neighbors. The first refinement for the meshes listed above would place new nodes at the midpoints of pairs 1,2 and 4,5. For pairs 2,3 and 3,4,  $\kappa$  specifies how closely new nodes will be placed to  $x = 1/2$ . If the current step-size between nodes 2 and 3 is  $h_0$ , then a node will be placed a distance of  $\kappa h_0$  from 3 rather than at  $\frac{1}{2}h_0$  as a uniform discretization would dictate. The same is true for pair 3,4. When  $\kappa = 1/3$ , the nine point mesh from one refinement will have nodes at  $x = \{0, 3/18, 6/18, 8/18, 9/18, 10/18, 12/18, 15/18, 1\}$ .

Table III.3: Asymptotic convergence rates and number of iterations for various  $\kappa$

Level	$\kappa = 1/2$		$\kappa = 2/5$		$\kappa = 1/3$		$\kappa = 2/7$	
	Rate	Iteration	Rate	Iteration	Rate	Iteration	Rate	Iteration
4	0.32	13	0.27	12	0.13	8	0.30	13
5	0.33	14	0.29	13	0.28	12	0.65	37
6	0.33	15	0.32	14	0.31	15	1.07	Diverge
7	0.32	16	0.32	15	0.32	16	1.53	Diverge
8	0.32	16	0.31	16	0.36	19	2.04	Diverge
9	0.32	17	0.32	17	0.49	26	2.60	Diverge
10	0.32	17	0.32	17	0.59	37	3.20	Diverge
11	0.32	18	0.32	18	0.69	52	3.86	Diverge
12	0.32	18	0.32	18	0.79	72	4.57	Diverge
13	0.32	19	0.32	19	0.88	136	5.34	Diverge
14	0.32	19	0.32	19	0.97	588	6.16	Diverge
15	0.32	20	0.32	20	1.06	Diverge	7.03	Diverge

Table III.3 shows the asymptotic convergence rate and number of iterations required to solve for a number of discretizations. For "large"  $\kappa$  values close to  $1/2$ , the MG solver converges uniformly regardless of level. The solver behaves nominally up to level 8 for  $\kappa = 1/3$ . Beyond that point, for smaller  $\kappa$  and higher levels, there is a deterioration in the MG solver's performance.

One potential source of error arises from widely discrepant step-sizes. Given  $\kappa$ , the  $m^{\text{th}}$  refinement will have a maximum step-size of  $h_{\max} = (1 - \kappa)(\frac{1}{2})^{m+1}$  adjacent to the

boundary and a minimum step-size  $h_{\min} = \frac{1}{2}\kappa^{m+1}$  next to the point of interest at  $x = 1/2$ .

Defining the aspect ratio as  $r_a = \frac{h_{\min}}{h_{\max}}$ , it can easily be seen that  $r_a \rightarrow 0$  as  $m \rightarrow \infty$ . Although we care little of the aspect ratio's limit behavior, we do care how small it becomes through a typical number of refinements. Table III.4 shows the aspect ratio for different  $\kappa$  through 10 refinements. It seems plausible that the widely discrepant step-sizes generate a

Table III.4: Aspect Ratio and min/max step-size after 10 refinements

$\kappa$	1/2	2/5	1/3	1/4	1/5	1/10
$h_{\min}$	2.44 E-04	2.10 E-05	2.82 E-06	1.19 E-07	1.02 E-08	5.00 E-12
$h_{\max}$	2.44 E-04	2.93 E-04	3.26 E-04	3.66 E-04	3.91 E-04	4.39 E-04
$a_r$	1	7.16 E-02	8.67 E-03	3.26 E-04	2.62 E-05	1.14 E-08

matrix that is incapable of reconciling error at different frequencies within the same mesh. This problem is exacerbated as the grading ratio is made more aggressive and the number of refinements increase. The aspect ratio will be a useful proxy to classify this behavior.

It is not all bad news though. Our MG solver performs nominally provided  $\kappa$  is not too aggressive. The failed attempts provide a better idea of where to look for the origin of our error. An interesting phenomenon we observed in our two-dimensional solver for the corner singularity problem is the genesis of oscillations along strongly graded grid-lines. In particular, instabilities seem to originate at nodes with highly discrepant step-sizes in the  $x$  and  $y$  directions. This behavior can be observed in Figure III.3 and precipitates divergence. Beyond the aesthetic value of the figure, it provides a hint concerning where within the system matrix to focus our attention.

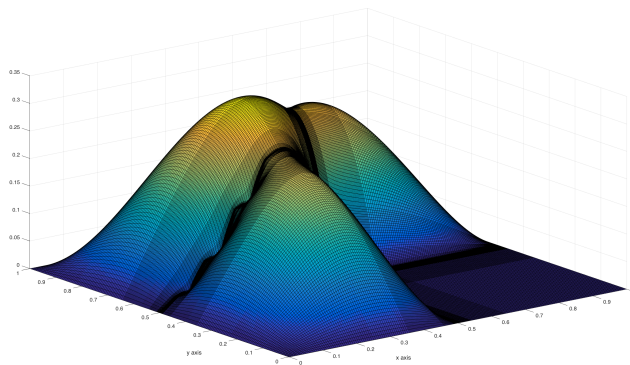


Figure III.3: Oscillations arising from highly irregular discretizations

## IV. FUTURE WORK

An obvious extension of our work in Chapter II is to establish upper bounds on the approximation error in three-dimensions and beyond. We have every reason to believe that a similar approach will provide an equivalent result, but have not yet worked through the details. We would also like to show that high dimension analogues of the Shortley-Weller equation yield  $O(h^2)$  approximations as well. The authors of [3] appear to have done so, but it is not clear from their paper that it holds for all cases or if it relies on the geometry of their domain. In addition, we would like to investigate high-order approximation schemes through the use of a nine-point, rather than five-point, stencil and show that there is no loss in its rate of convergence either.

On the numerical front discussed in Chapter III, our immediate goal is to develop a stable fast-solver for non-uniform discretizations. A potential source of the solver's divergent behavior might be our prolongation routine which dictates how correction values are mapped from coarse-to-fine grids. Since the minimum step-size quickly shrinks with aggressive grading, round-off error becomes a concern making accurate mappings between grids essential. Beyond linear interpolation, we have tried quadratic interpolation and the use of cubic splines. To this point, all attempts have failed to prevent divergence; some have delayed it, but not effectively enough to justify the additional complications in our algorithm.

Although we have attempted several prolongation schemes, there are many others that are worth investigating. Other potential corrective measures include block GS smoothing, successive over relaxation (SOR), and higher precision data types. The first order of business, however, is to develop a better understanding of why the solver fails to converge. To this end, work is currently underway to quantify the amount of asymmetry in the system matrix as a function of  $\kappa$ . Our hope is to establish a threshold level of asymmetry, below which the solver converges, then look for ways to increase it.

At this point, it is unclear whether we can expect uniform convergence with the proposed solver for aggressive grading ratios. Once the divergent behavior of our solver has been classified, it will be easier to understand where the breakdown occurs.

## REFERENCES

- [1] Bramble, J.H. and Hubbard, B.E. "On the Formulation of finite Difference analogues of the Dirichlet Problem for Poisson's Equation." *Numerische Mathematik* 4.1 (1962): 313-327.
- [2] Collatz, Lothar. *The numerical treatment of differential equations* (Berlin: Springer, 1966, 3rd ed. 1960), pg. 46.
- [3] Min, Chohong, Frédéric Gibou, and Hector D. Ceniceros. "A supra-convergent finite difference scheme for the variable coefficient Poisson equation on non-graded grids." *Journal of Computational Physics* 218.1 (2006): 123-140.
- [4] Shortley, George H., and Royal Weller. "The numerical solution of Laplace's equation." *Journal of Applied Physics* 9.5 (1938): 334-348.